ACCOUNTS
of chemical research

Redox Potentials and Acidity Constants from Density Functional Theory Based Molecular Dynamics

Jun Cheng,*,[†,‡] Xiandong Liu,[‡,¶] Joost VandeVondele,[§] Marialore Sulpizi,[∥] and Michiel Sprik*,[‡]

[†]Department of Chemistry, University of Aberdeen, Aberdeen AB24 3UE, United Kingdom
[‡]Department of Chemistry, University of Cambridge, Cambridge CB2 1EW, United Kingdom
[¶]State Key Laboratory for Mineral Deposits Research, School of Earth Sciences and Engineering, Nanjing University, Nanjing 210093, People's Republic of China
[§]Department of Materials, ETH Zurich, Wolfgang-Pauli-Strasse 27, CH-8093 Zurich, Switzerland
[∥]Department of Physics, Johannes Gutenberg Universitat, Staudingerweg 7, 55099, Mainz, Germany

Ⓢ *Supporting Information*

CONSPECTUS: All-atom methods treat solute and solvent at the same level of electronic structure theory and statistical mechanics. All-atom computation of acidity constants (pK_a) and redox potentials is still a challenge. In this Account, we review such a method combining density functional theory based molecular dynamics (DFTMD) and free energy perturbation (FEP) methods. The key computational tool is a FEP based method for reversible insertion of a proton or electron in a periodic DFTMD model system. The free energy of insertion (work function) is computed by thermodynamic integration of vertical energy gaps obtained from total energy differences. The problem of the loss of a physical reference for ionization energies under periodic boundary conditions is solved by comparing with the proton work function computed for the same supercell. The scheme acts as a computational hydrogen electrode, and the DFTMD redox energies can be directly compared with experimental redox potentials.

Consistent with the closed shell nature of acid dissociation, pK_a estimates computed using the proton insertion/removal scheme are found to be significantly more accurate than the redox potential calculations. This enables us to separate the DFT error from other sources of uncertainty such as finite system size and sampling errors. Drawing an analogy with charged defects in solids, we trace the error in redox potentials back to underestimation of the energy gap of the extended states of the solvent. Accordingly the improvement in the redox potential as calculated by hybrid functionals is explained as a consequence of the opening up of the bandgap by the Hartree−Fock exchange component in hybrids. Test calculations for a number of small inorganic and organic molecules show that the hybrid functional implementation of our method can reproduce acidity constants with an uncertainty of 1−2 pK_a units (0.1 eV). The error for redox potentials is in the order of 0.2 V.
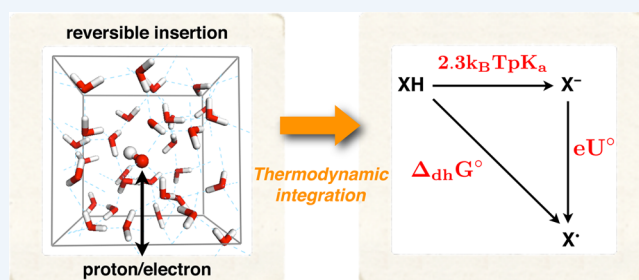
■ INTRODUCTION

Redox potentials and acidity constants (pK_a's) are two of the most fundamental quantities in solution chemistry determining the thermochemistry of electron and proton transfer reactions. Solvation effects are commonly described by implicit solvent models[1,2] or a distribution of point dipoles.[3] Modeling the solvent with a dielectric continuum gains efficiency, while sophisticated parametrization procedures ensure accuracy. The combination of these two explains the impressive success of this approach in calculating the equilibrium constants of electron/proton transfer reactions in aqueous solution. If needed QM/MM methods can add further atomic detail replacing some or all of the continuum solvent by an atomistic classical force field model.[4,5]

The alternative is a fully consistent first-principles "all-atom" method treating solute and solvent at the same level of electronic structure theory. This is the topic of the present Account. We review an all-atom method using the density functional theory based molecular dynamics (DFTMD) implementation in the CP2K package[6,7] as the key numerical tool. Energies sampled from a DFTMD trajectory are used as input for a free energy perturbation (FEP) scheme[8] and converted to work functions for reversible removal of electrons and protons from the DFTMD model system. The method was developed in a series of computations of redox potentials and pK_a's of various simple aqueous species.[9−13] Electronic polarization of both solute and solvent is included at a fundamental level. In addition, the DFTMD method captures the statistical mechanical nature of solvent fluctuations and consistently accounts for the motion of the first solvation shell and the interaction with the bulk solvent. The obvious

downside of DFTMD is the computational cost. However, thanks to ever-increasing computer power and the development of efficient computing algorithms, it is now feasible to run free energy calculations using DFTMD in model systems consisting of a few hundred atoms. This is sufficient for investigations of many interesting systems including bulky solutes[11,12,14−17] and even solid−liquid interfaces.[18−25]

While explicitly represented in a DFTMD simulation, electronic polarization, specific hydrogen bonding, and thermal fluctuations are classical solvation effects that ideally can be reproduced by implicit solvent and QM/MM methods. However, the DFTMD approach also allows for hybridization of the localized electronic states of the redox active solutes with the extended band states of the solvent. This feature is unique to DFTMD. Unfortunately it exposes DFTMD to the infamous delocalization error in its most vicious form, known as the bandgap error,[26] leading to significant underestimation of redox potentials.[13] We became aware of this problem only recently when it became possible to carry out DFTMD simulation using hybrid functionals containing a fraction of Hartree−Fock exchange (HFX).[27]

In addition to the enhancement of the delocalization error, DFTMD has to face further complications that are of no or little concern for implicit solvent models. DFTMD simulations of liquids apply periodic boundary conditions (PBC). However, ionization of a solvated species creates ions. The long-range electrostatic interactions between these ions and their periodic images are spurious and another source of computational bias. Finally there is of course also the issue of statistical uncertainty of the sampling and limitations in the time scale for the relaxation (reorganization) of the solvent. It is very hard to separate these effects. We have made however some progress and are now at least able to assess the relative severity of each of these sources of error.

DFTMD model systems are small. A typical supercell is cubic with a side L between 10 and 12 Å. Corrections for finite system size errors have a long history in computational solid state physics of charged defects in semiconductors and insulators[28] with a parallel development in computational solution chemistry.[29,30] The solid state physics community has reached a consensus how to deal with finite size errors in formation energies of charged defects.[31,32] While it should be possible to adapt these methods to correct solvation free energies of ions in solution, the state of the art in computational solution chemistry still relies on the seminal work by Hummer et al., who pointed out that for monovalent ions the finite size errors as obtained in Ewald summation methods are surprisingly small.[29,33] The powerful dielectric screening properties of water eliminate the leading $1/L$ term. For example, for OH^-, the finite size error in a 10 Å cubic box is only 0.1 eV.[11,33]

Ewald summation acts as a boundary condition at infinity setting the average electrostatic potential to zero.[29] This is a second supercell effect that should be distinguished from the interaction between periodic images. The uncertainty in the "zero" of the electrostatic potential has no effect on the total energy of a neutral system, but for the calculation of ionization energies, the zero of the electrostatic potential must be explicitly aligned to an external reference. The standard procedure in computational solid state physics is to introduce an interface with vacuum.[31] With some effort, this calculation can also be carried out for liquid water.[34] Our approach is to stay close to electrochemistry and use the work function of the

proton as reference.[35] The work function as computed using the reversible proton insertion technique is subject to the same bias as electronic ionization energies but with the opposite sign.[11,12,20] In fact when referred to the work function of the proton, ionization energies can be directly represented as potentials on the standard hydrogen electrode (SHE) scale.[35]

Reversible insertion of protons is computationally more involved (and expensive) than addition and removal of electrons. However, reversible proton insertion can be used to estimate acidity constants as well. We regard consistent treatment of ionization and deprotonation as absolutely crucial for proton coupled electron transfer (PCET) reactions. PCET is a key mechanism for many redox reactions in organic, inorganic, and biological systems.[36] From a technical point of view, the comparison of free energy changes of PCET reactions is a strong test for our method. Hess's law requires dehydrogenation energies to be equal to the sum of the corresponding deprotonation and oxidation energies. Our calculations show that Hess's law is indeed satisfied within 0.1 eV, setting a measure for the statistical uncertainty in the computed redox potentials and pK_a's.
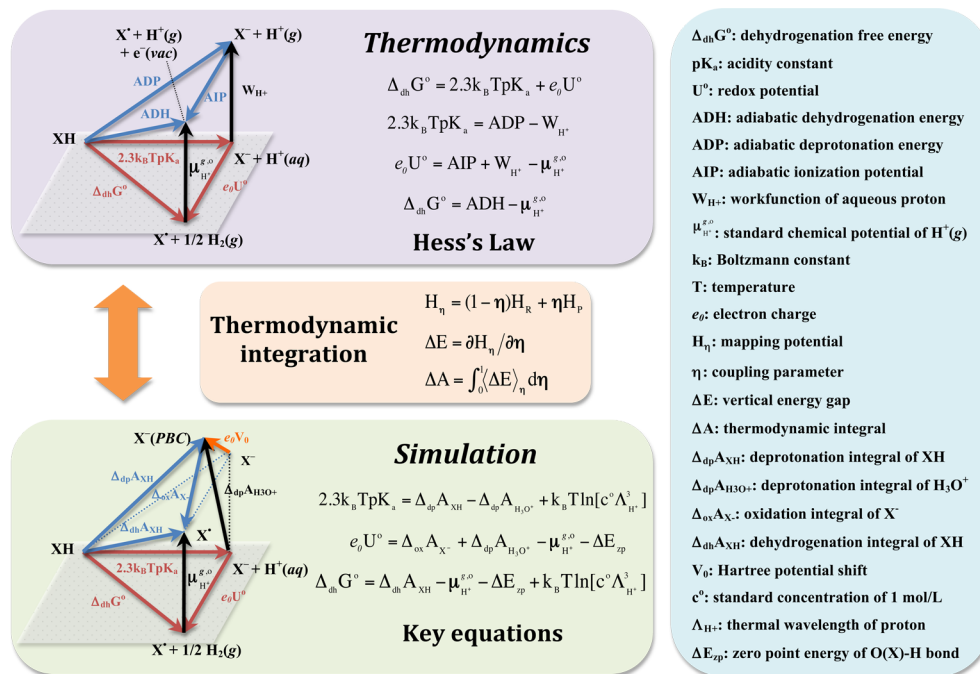
The conclusion is that the uncertainty due to limitations in system size and sampling time in redox potentials and acidity constants of the small aqueous species studied in ref 13 is no more than 0.2 eV. This margin is sufficiently tight for a proper assessment of errors due to the shortcomings in the DFT approximation. The functionals commonly used in DFTMD are based on the generalized gradient approximation (GGA). We found that the computed pK_a's were accurate with an uncertainty of 1−2 pK units (0.15 eV). The computed redox potentials, on the other hand, are systematically underestimated. The size of the error varies, and for highly oxidative couples, the error can be very large, for example, 0.9 eV for $Cl^-/Cl^{\bullet}$.[13]

The contrast in performance of the GGA for pK_a and redox potential calculation was for us a confirmation that the large errors in redox potentials are to blame in the delocalization error. Acid dissociation is closed shell chemistry, which is much less sensitive to the delocalization error than the open shell radicals created by oxidation. Drawing a parallel with computational solid state defect physics,[31,37] we were also able to rationalize why misalignment of the band states of the solvent aggravates the error. Indeed the improvement brought about by hybrid functionals is largely the result of the opening of the band gap, which is a well-known effect of the introduction of HFX.

In this Account, we will briefly recapitulate our method for computation of redox potentials and acidity constants. The emphasis will be on the idea of the computational SHE and how to relate the computed thermodynamic integrals with pK_a's and redox potentials vs SHE. Then, we will review the previously reported results mainly calculated using GGAs and also present some new results computed using hybrid functionals. Critical error analysis will be carried out to demonstrate how the delocalization error in GGAs affects redox potentials. The improvement by hybrid functionals reinforces this claim. We will end this Account with some conclusions and an outlook.
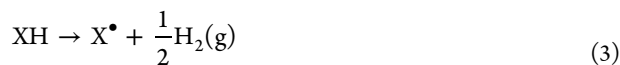
■ METHOD

Consider the acid dissociation of a hydride XH and subsequent oxidation of its anion X^-

Scheme 1. Schematic Representation of the Method for Computation of Redox Potentials and Acidity Constants[a]

Thermodynamics

$$\Delta_{dh}G^\circ = 2.3k_B TpK_a + e_0 U^\circ$$

$$2.3k_B TpK_a = ADH - W_{H^+}$$

$$e_0 U^\circ = AIP + W_{H^+} - \mu_{H^+}^{g,o}$$

$$\Delta_{dh}G^\circ = ADH - \mu_{H^+}^{g,o}$$

Hess's Law

Thermodynamic integration

$$H_\eta = (1-\eta)H_R + \eta H_P$$

$$\Delta E = \partial H_\eta / \partial \eta$$

$$\Delta A = \int_0^1 \langle \Delta E \rangle_\eta \, d\eta$$

Simulation

$$2.3k_B TpK_a = \Delta_{dp}A_{XH} - \Delta_{dp}A_{H_3O^+} + k_B T\ln[c^\circ\Lambda_{H^+}^3]$$

$$e_0 U^\circ = \Delta_{ox}A_{X^-} + \Delta_{dp}A_{H_3O^+} - \mu_{H^+}^{g,o} - \Delta E_{zp}$$

$$\Delta_{dh}G^\circ = \Delta_{dh}A_{XH} - \mu_{H^+}^{g,o} - \Delta E_{zp} + k_B T\ln[c^\circ\Lambda_{H^+}^3]$$

Key equations

$\Delta_{dh}G^o$: dehydrogenation free energy
pK_a: acidity constant
U^o: redox potential
ADH: adiabatic dehydrogenation energy
ADP: adiabatic deprotonation energy
AIP: adiabatic ionization potential
W_{H^+}: workfunction of aqueous proton
$\mu_{H^+}^{g,o}$: standard chemical potential of $H^+(g)$
k_B: Boltzmann constant
T: temperature
e_0: electron charge
H_η: mapping potential
η: coupling parameter
ΔE: vertical energy gap
ΔA: thermodynamic integral
$\Delta_{dp}A_{XH}$: deprotonation integral of XH
$\Delta_{dp}A_{H3O^+}$: deprotonation integral of H_3O^+
$\Delta_{ox}A_{X^-}$: oxidation integral of X^-
$\Delta_{dh}A_{XH}$: dehydrogenation integral of XH
V_0: Hartree potential shift
c^o: standard concentration of 1 mol/L
Λ_{H^+}: thermal wavelength of proton
ΔE_{zp}: zero point energy of O(X)-H bond

[a]The red triangle in the top left panel represents the reactions, eqs 1−3. The blue triangle is the result of a change of the reference state for hydrogen to the gas-phase proton as indicated by the black arrows. The middle panel summarizes the key equations in the free energy calculation. The bottom left panel shows how pK_a's and redox potentials vs SHE are related to the computed thermodynamic integrals. The blue dotted triangle corresponds to the blue triangle in the top panel. In the calculation, it is replaced by the solid blue triangle in the bottom panel because of the uncertainty in the potential reference under PBC, as denoted by the orange arrow. Symbols are defined in the right panel. For $\mu_{H^+}^{g,o}$, we use the experimental value of 15.81 eV. The two correction terms, ΔE_{zp} and $k_B T\ln[c^\circ\Lambda_{H^+}^3]$, are 0.35 and −0.19 eV, respectively.

$$XH \rightarrow X^- + H^+(aq) \tag{1}$$

$$X^- + H^+(aq) \rightarrow X^\bullet + \frac{1}{2}H_2(g) \tag{2}$$
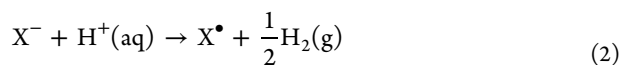
$H^+(aq)$ is the reference ion for both the acidity and SHE scale. The free energy of reaction 1 is therefore equal to $2.3k_B TpK_a$ and that of reaction 2 to $e_0 U^\circ$ where U° is the standard potential vs the SHE. Summing gives the dehydrogenation reaction,

$$XH \rightarrow X^\bullet + \frac{1}{2}H_2(g) \tag{3}$$

The dehydrogenation free energy denoted by $\Delta_{dh}G^\circ$ should be equal to the sum of $2.3k_B TpK_a$ and $e_0 U^\circ$ (Hess's law).

The FEP method to compute these energies has been presented in detail in previous publications[11,12,20] and is summarized in Scheme 1. Reactions 1, 2, and 3 are represented by the red triangle. Changing the reference ion from the aqueous to the gas-phase proton creates a new PCET triangle indicated in blue. The proton has been taken out of solution $(H^+(aq) \rightarrow H^+(g))$ and the gas-phase hydrogen molecule has been dissociated $(^1/_2 H_2(g) \rightarrow H^+(g) + e^-(vac))$. These reactions are indicated by black arrows. The corresponding reaction free energies are the work function of the aqueous proton (W_{H^+}) and standard chemical potential of the gas phase proton $(\mu_{H^+}^{g,o})$. The free energies of the reactions in the blue triangle are the adiabatic deprotonation energy (ADP), ionization potential (AIP), and dehydrogenation energy (ADH). The equations relating the free energies of the red and blue triangle are given on the right of the diagram. The symbols used in this Account are defined in the right panel.

The energies computed by the FEP method are the insertion energies of the blue triangle. A fictitious mapping Hamiltonian $H_\eta = (1 - \eta)H_R + \eta H_P$ is constructed by superimposing the Hamiltonians H_R of reactant and H_P of the product state.[8] The coupling parameter η connecting the reactant and product states takes the values 0 to 1. The coupling parameter derivative of H_η is the energy difference between the reactant and product states at a fixed configuration. This quantity, called the vertical energy gap, ΔE, is obtained from the electronic structure calculation as a total energy difference. The vertical energy gap is averaged over molecular dynamics (MD) runs for a sequence of values of η. Integration of the thermal average $\langle \Delta E \rangle_\eta$ converts vertical into adiabatic ionization energies (see the middle panel of Scheme 1 for key equations).

The FEP scheme amounts to reversible deletion of a proton (eq 1), electron (eq 2), or both (eq 3). Addition and removal of an electron can be simply implemented by adjusting the number of electrons and reoptimizing the electronic state. The same applies to removal of a proton, but addition of proton can cause problems when the location of the insertion is too close to a nearby atom. To avoid this problem, the acid proton is not fully eliminated from the system. Instead its charge is switched off and on. During the off stage, when the proton is invisible to the nuclei and electrons, it is kept in place by a harmonic restraining potential preventing overlap with other nuclei.[10,11,38] The resulting ionization integrals are denoted by $\Delta_{dp}A_{XH}$ for deprotonation and $\Delta_{ox}A_{X^-}$ for oxidation. The work function, W_{H^+}, of the proton is approximated by the deprotonation free energy, $\Delta_{dp}A_{H_3O^+}$ of the hydronium ion.

Because of the uncertainty in the reference of the electrostatic potential $\Delta_{dp}A_{XH}$ and $\Delta_{ox}A_{X^-}$ are *not* yet equal to

Table 1. Deprotonation Integrals (ΔA) and Conversion to the Free Energies (ΔG) and pK_a's of the Corresponding Acid Dissociation Reactions Compared with the Experimental Values[a]

deprotonation	GGA/BLYP			hybrid/HSE06			expt	
	ΔA	ΔG	pK_a	ΔA	ΔG	pK_a	ΔG	pK_a
$H_3O^+ \rightarrow H_2O$	15.35	−0.19	−3.2	15.29	−0.19	−3.2	−0.10	−1.7
$H_2O(l) \rightarrow OH^-$	16.34	0.70	11.9	16.29	0.71	12.0	0.83	14.0
$H_2O_2 \rightarrow HO_2^-$	16.11	0.57	9.7	16.09	0.61	10.3	0.69	11.7
$HO_2^\bullet \rightarrow O_2^{\bullet-}$	15.73	0.19	3.2	15.74	0.26	4.4	0.21	3.6
$HCl \rightarrow Cl^-$	15.1	−0.4	−7.5				−0.41	−7.0
$HCOOH \rightarrow HCOO^-$	15.8	0.3	4.4				0.22	3.8
$NH_4^+ \rightarrow NH_3$	16.2	0.7	11.2				0.54	9.2
$H_2S \rightarrow HS^-$	16.0	0.5	7.8				0.41	7.0
$HS^- \rightarrow S^{2-}$	16.5	1.0	17.1				1.0	17
$CH_3SH \rightarrow CH_3S^-$	16.2	0.7	11.2				0.61	10.3
PheA	16.3	0.8	12.9				0.80	13.5
PheB	16.1	0.6	9.5				0.55	9.3
$H_2Q \rightarrow HQ^-$	16.20		8.6				0.58	9.8
$H_2Q^{\bullet+} \rightarrow HQ^\bullet$	15.76		1.2				−0.06	−1.0
$HQ^\bullet \rightarrow Q^-$	15.94		4.2				0.24	4.1
$HQ^+ \rightarrow Q$	15.23		−7.8				−0.41	−6.9
$TyrOH \rightarrow TyrO^-$	15.78		9.3				0.60	10.1
$TrpH^{\bullet+} \rightarrow Trp^\bullet$	15.54		5.2				0.25	4.3
MUE		0.07	1.0		0.09	1.4		
MAE		0.01	−0.1		−0.06	−1.0		

[a]PheA and PheB are two substituted phenols; Q stands for quinone. References to the original papers are given in the text. All the energies are in eV.

the ADP and AIP that we want to calculate.[11] As indicated by an orange arrow in the bottom left panel of Scheme 1, the energy of an anion X^- under PBC is shifted by an unknown energy e_0V_0. Here is where our computational SHE comes in. The deprotonation integral of aqueous hydronium ($\Delta_{dp}A_{H_3O^+}$) differs from the experimental W_{H^+} by the same e_0V_0. The acidity is the difference of the ADP of the acid and the hydronium, which can be estimated by subtracting $\Delta_{dp}A_{H_3O^+}$ from $\Delta_{dp}A_{XH}$ as indicated in the lower panel of Scheme 1. The e_0V_0 cancels out. Similarly the redox free energy e_0U° can be calculated by adding $\Delta_{ox}A_{X^-}$ and $\Delta_{dp}A_{H_3O^+}$. The dehydrogenation integral $\Delta_{dh}A_{XH}$ is already invariant under a change of reference potential and $\Delta_{dh}G^\circ$ is calculated by simply adding $\Delta_{dp}A_{XH}$ and $\Delta_{ox}A_{X^-}$.

This is the essence of the DFTMD/FEP calculation of the pK_a, e_0U°, and $\Delta_{dh}G^\circ$. For the final result, two correction terms have to be included (see again Scheme 1). ΔE_{zp} is a correction for the zero point energy of the inserted proton, which is treated as a classical particle in DFTMD.[11] The $k_BT \ln[c^\circ\Lambda_{H^+}^3]$ term adds in the free energy related to the translational entropy generated by the acid dissociation.[12]

ASSESSMENT

Tables 1−3 give a selection of results of previous publications.[10−16] We have included the thermodynamic integrals, ΔA, which substituted into the key equations in Scheme 1 yield the pK_a's, redox potentials vs SHE, and dehydrogenation energies, which can be directly compared with experiment (see our previous publications for references). An example of calculating the dehydrogenation integral of water ($\Delta_{dh}A_{H_2O}$) is given in Figure S1 in the Supporting Information.

$\Delta_{dp}A_{H_3O^+}$ is the reference integral that is required in all the conversions.

Table 2. Oxidation Integrals (ΔA) and Corresponding Redox Potentials (U°) Compared with Experiment[a]

oxidation	GGA/BLYP		hybrid/HSE06		expt
	ΔA	U°	ΔA	U°	U°
$OH^- \rightarrow OH^\bullet$	2.1	1.3	2.52	1.65	1.90
$HO_2^- \rightarrow HO_2^\bullet$	1.1	0.3	1.33	0.46	0.75
$O_2^{\bullet-} \rightarrow O_2$	0.3	−0.5	0.52	−0.35	−0.16
$Cl^- \rightarrow Cl^\bullet$	2.3	1.5	2.73	1.87	2.41
$HS^- \rightarrow HS^\bullet$	1.3	0.5	1.71	0.84	1.08
$CO_2^{\bullet-} \rightarrow CO_2$	−1.26	−2.07	−1.09	−1.96	−1.90
$H_2Q \rightarrow H_2Q^{\bullet+}$	1.12	0.40			1.10
$HQ^- \rightarrow HQ^\bullet$	0.54	−0.12			0.46
$HQ^\bullet \rightarrow HQ^+$	1.23	0.57			0.76
$Q^{\bullet-} \rightarrow Q$	0.48	−0.18			0.10
$TyrO^- \rightarrow TyrO^\bullet$	1.28	0.16			0.72
$TrpH \rightarrow TrpH^{\bullet+}$	1.53	0.41			1.15
MUE		−0.51		−0.26	
MAE		0.51		0.26	

[a]The hybrid functional used to calculate CO_2 is PBE0. All the energies are in eV, and redox potentials are in V vs SHE.

The BLYP approximation is the functional of choice in DFTMD simulation of aqueous systems and was also the functional used in all calculations until the efficient algorithm for calculation of HFX became available in CP2K.[27] Using this method we have recalculated some of the integrals using the hybrid functionals HSE06[39] and PBE0.[40] These results are new and also listed in the tables. No finite size corrections have been applied because they can be assumed to be minimal for free energies for ions of low charge[11,33] (see also Introduction).

Before discussing the comparison to experiment, we first check the intrinsic consistency of our calculations. Hess's law requires the dehydrogenation integrals to be equal to the sum of the deprotonation and oxidation integrals, regardless of uniform shifts in ionization potentials, finite size, and DFT

Table 3. Dehydrogenation Integrals (ΔA) and Dehydrogenation Free Energies (ΔG) Compared with Experiment[a]

dehydrogenation	GGA/BLYP		hybrid/HSE06		expt
	ΔA	ΔG	ΔA	ΔG	ΔG
$H_2O(l) \rightarrow OH^{\bullet}$	18.54	2.10	18.89	2.45	2.72
$H_2O_2 \rightarrow HO_2^{\bullet}$	17.19	0.84	17.43	1.08	1.44
$HO_2^{\bullet} \rightarrow O_2$	16.16	−0.19	16.27	−0.08	0.05
$H_2Q \rightarrow HQ$	16.83	0.50			1.04
$HQ^{\bullet} \rightarrow Q$	16.57	0.24			0.35
$TyrOH \rightarrow TyrO^{\bullet}$	16.91	0.59			1.32
$TrpH \rightarrow Trp^{\bullet}$	17.21	0.89			1.41
MUE		−0.48		−0.26	
MAE		0.48		0.26	

[a]The liquid is used as standard state for water. All the energies are in eV.

errors. It is also a strong check for the statistical accuracy. According to Tables 1−3, all our calculations satisfy Hess's law within 0.1 eV.

The overall errors are indicated by the mean unsigned error (MUE) and mean signed error (MAE). The calculation reproduces the experimental pK_a's at a high accuracy. The error is within 0.1 eV, comparable to the size of the statistical error (Table 1). Both BLYP and hybrid functionals perform well over the full range of 20 pK_a units covered by the model acids we investigated. This is encouraging. It is strong evidence that the deprotonation integrals including the reference integral, $\Delta_{dp}A_{H_3O^+}$ are insensitive to details of the density functional approximation and may therefore not suffer from the delocalization error. Also, the accuracy of the pK_a calculation is

support of our claim that finite size errors are small. The errors in redox potentials are much larger. For BLYP, the error is 0.5 V reduced by half by HSE06. Redox potentials are consistently underestimated as implied by the same magnitude of MUE and MAE. The reference $\Delta_{dp}A_{H_3O^+}$ is essentially the same for BLYP and HSE06. The error can therefore only stem from the oxidation integrals. Finally, the errors in the dehydrogenation energies are similar to the errors in the redox potentials. This is expected because restrained by Hess's law, the dehydrogenation energies have to inherit the errors in the redox potentials.

■ ENERGY LEVEL DIAGRAMS

Energy level diagrams are a convenient way of analyzing ionization potentials. Particularly instructive are diagrams combining *adiabatic* and *vertical* levels. Adiabatic levels are thermodynamic energy levels; $-e_0U^{\circ}$ plays this role in redox chemistry. A vertical level is obtained when the electron detachment/attachment takes place without allowing for ionic reorganization. There are therefore two vertical levels, minus the vertical ionization potential of the equilibrated reduced state (IP_R) and the minus vertical electron affinity of the equilibrated oxidized state (EA_O). The differences between adiabatic and vertical energies are the reorganization energies, λ_O in the oxidized state and λ_R in the reduced state. If the solvent response is linear, as assumed in Marcus theory, $\lambda_O = \lambda_R$. As a result, $eU^{\circ} = 1/2(IP_R + EA_O)$. The redox level is midway between the $-IP_R$ and $-EA_O$ level.

The FEP method converts vertical to adiabatic energies by a coupling parameter integral. The end points of this integral are physical and are the vertical energies that we need for the level diagram. Specifically, $\langle \Delta E \rangle_{\eta=0} = IP_R$ and $\langle \Delta E \rangle_{\eta=1} = EA_O$. Similarly the computational hydrogen electrode can be used to
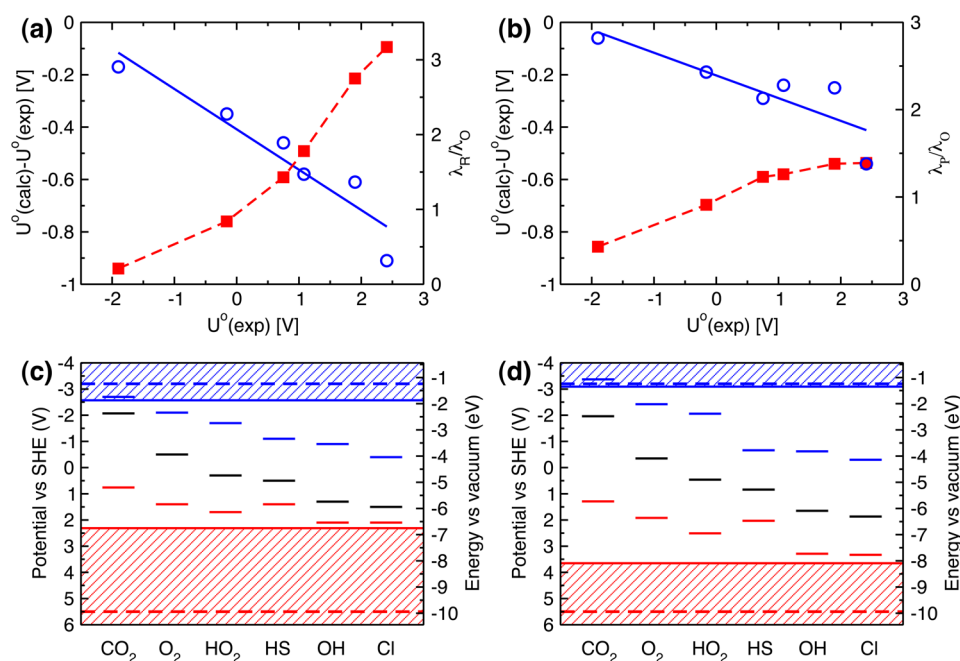
Figure 1. Errors in the redox potential calculation (a, b) and level alignment (c, d) for six aqueous species using GGA (a, c) and hybrid functionals (b, d). In panels a and b, the blue circles stand for the difference of the computed redox potentials and the experimental estimates plotted against the experimental estimates. The blue lines are linear fits. The asymmetry in reorganization energies are shown as the ratio λ_R/λ_O (red squares). In panels c and d, the short black, blue, and red lines correspond to the computed redox potentials, vertical electron affinities of oxidized states, and vertical ionization potentials of reduced states, respectively. The shaded areas in blue and red show the calculated conduction bands and valence bands of water, respectively. The long dashed lines indicate the experimental CBM and VBM.
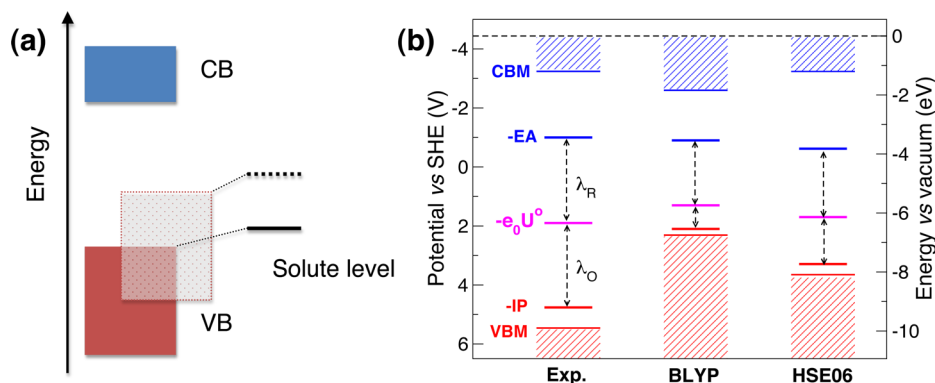
Figure 2. (a) Schematic representation of how the solvent band states affect solute energy levels. The tranparent rectangle stands for the valence band moved up by the delocalization error in density functional approximations. This turns a solute level in the gap (black level on the right) into a resonant impurity generating a shallow defect level (dotted line) just above the misaligned valence band. (b) Energy levels of the OH$^\bullet$/OH$^-$ couple aligned with the band edges of water.[13]

align adiabatic as well as verticals levels to the SHE. The offset is the same. The BLYP and HSE06 levels obtained by this procedure are listed in Table S1 in the Supporting Information.

Also relevant are the conduction band minimum (CBM) and valence band maximum (VBM) of liquid water. Their positions can be obtained from the IP or EA of the pure liquid calculated by either using total energy differences or Kohn−Sham orbital energies. For extended states, these two should be identical even though both can be incorrect due to the band edge error.[26,37] This is indeed the case for water as shown in Table S2 in the Supporting Information (see also refs 20 and 34).

The computed vertical and adiabatic levels are plotted together with the band edges of water in Figure 1. The underestimation of redox potentials shows a linear correlation with the redox potentials (blue lines in Figure 1a,b); The error is larger for more positive redox potentials. The improvement of HSE06 over BLYP is manifested in the reduced slope of the linear fit. There is a clear asymmetry in the reorganization energies for BLYP with the λ_R/λ_O ratio (red squares in Figure 1a,b) varying from 0.2 to 3.2. Changing to HSE06 alleviates the asymmetry but only at the positive end of the redox potential interval. When we compare the levels in Figure 1c,d, the maximum discrepancy between BLYP and HSE06 is the position of the $-IP_R$ level at high potential and, related to this, the different λ_R/λ_O ratios.

■ COUPLING TO BAND STATES

Water is a wide gap insulator. In fact the experimental band gap of liquid water (8.7 eV) is close to that of solid SiO$_2$. DFT calculation of charge transition levels (redox potentials) of point defects in main group oxides such as SiO$_2$ or MgO have already a long and rather frustrating history with large discrepancies between various levels of DFT approximations and experiment.[31,37] A breakthrough was made when it was realized that the energy of midgap levels when aligned with an external reference (ideally vacuum), rather than with the VBM, are actually reproduced rather well by DFT. It was the position of the VBM itself that was wrong. Moreover it was established that the errors in charge transition levels increase when the level approaches the band edges (shallow defects) showing that the mixing with the misaligned band states is a source of error. This raises the question whether the band states of water in Figure 1 could have a similar effect.

The parallel is suggestive. Just as with other main group oxides, DFT for liquid water suffers from a severe band gap problem. The GGA underestimates the bandgap by almost 4 eV (see Table S2 in the Supporting Information). The VBM, consisting of O 2p levels, is placed ∼3.5 eV too high, while the position of the CBM is ∼0.5 eV too low (see Figure 1). The band gap error is therefore basically due to underestimation of the ionization potential. This effect is also reflected in the opening up of the band gap by HSE06. It does so mainly by pushing down the VBM. However, HSE06 does not quite make it. The residual error in the VBM position is still about 2 eV. The CBM is lifted ending up almost at the right energy. PBE0 further increases the band gap by ∼0.6 eV, but this improvement is not the result of lowering the VBM but underestimating the vertical electron affinity (For a GW perspective, see ref 34.).

A shallow acceptor state near the VBM can hybridize with the extended band states of the host repelling the level. In a worst case scenario, a localized defect level can be overtaken by the VBM and become a resonant impurity state.[31] This could be the fate of a radical such as Cl$^\bullet$ or OH$^\bullet$ produced by vertical ionization. The ionizable orbitals of the corresponding anions have a similar lone pair p-orbital character as the states making up the top of the valence band of water. The resonance generates a new defect level above the VBM as illustrated in Figure 2a. In any case a shallow defect level will follow the destabilized VBM to more negative reduction potentials. The delocalization error in the GGA destabilized the water VBM by as much as 3.5 eV. The error is passed on to p-like solute levels although in a somewhat mitigated form. This is shown in Figure 2b for OH$^\bullet$/OH$^-$.[13]

Note that hybridization between solute levels and band states can be a *real* effect. The GGA exaggerates by pushing up the water VBM. Looking at the negative end of the potential interval in Figure 1, we see that the GGA gives a good redox potential for CO$_2$/CO$_2^-$ even in the presence of mixing of the $-EA_O$ level and the conduction band of water, as manifested by the asymmetry in reorganization energies. Recall that the CBM is at about the correct energy. This hybridization effect is most likely real and underlines the significance of the band structure of water in describing aqueous species.

HFX is known to increase the band gap. Normally the CBM moves up by as much as the VBM moves down.[37] However, hybrid functionals seem to be an exception at least in the case

liquid water. As illustrated in Figure 2b, HSE06 pushes down the VBM. The effect on the CBM is much more modest. The result is a significant decrease in the error in the $-IP_R$ and redox level of the $OH^\bullet/OH^-$. PBE0 shows a similar effect (see Table S3 in the Supporting Information; note that CP2K truncates PBE0 to fit in the supercell).

Increasing the fraction of HFX is a device that has been successfully used to adjust the charge transition levels in solids.[31,37] To see whether this also works for water, we have calculated the redox potential of the $OH^\bullet/OH^-$ couple using PBE0 with 0.37 and 0.5 HFX. It is somewhat surprising to see that the results get worse. Structural analysis indicates that with too much HFX the solvation structure becomes unstable. For example, we find that the effective number of H-bonds of the O atom in $OH^\bullet$ decreases from 1.7 to 1.3 and 1.1 with increasing HFX mixing. Coordination is more labile in liquids than in solids making the minimization of the error in redox potentials a rather more delicate affair.

Finally, we comment on the issue of potential alignment. In experimental solid state physics, defect levels are often referred to band edges. From the perspective of DFT, this is not a good choice. Other references such as core electron levels and averaged electrostatic potentials are preferred.[37] The advantage of our SHE is that the reference energy against which we compare, $\Delta_{dp}A_{H_3O^+}$, can be accurately calculated in the GGA and is practically insensitive to details of density functionals. We recapitulate that $\Delta_{dp}A_{H_3O^+}$ is composition dependent and must be recomputed for every supercell. With this caveat, the scheme is general and can also be used for the alignment of energy levels across electrochemical interfaces.[20]

CONCLUSION

We have summarized the DFTMD/FEP method that we have developed for computation of aqueous redox potentials and acidity constants. The overall error for acidity constants is within $1-2$ pK_a units even at the GGA level. The error for redox potentials is much larger, particularly for species with high redox potentials. Consistency of acidity constant and redox potential calculations was a crucial concern in the design of the method. This allowed us to attribute the poor performance for redox potentials to the delocalization error. Indeed, hybrid functionals significantly improve on the GGA, reducing the error to ~0.2 eV.

This level of accuracy should be sufficient for many applications in aqueous chemistry (e.g., geochemistry), but care should be taken when the vertical levels of solutes approach the band edges of water. Another important application area is interfacial electrochemistry, especially for semiconductor electrodes with medium band gaps where HSE06 gives good band alignment. Further improvement requires eliminating the residual delocalization error, in particular lowering the VBM of water to the correct position. A promising way is to use many body perturbation methods, for example, GW[34,41] or MP2 and RPA[42,43] Finally, the combination of computation of redox potentials and acidity constants allows for calculating the thermochemistry of PCET. This is expected to be a fruitful application direction becauseee PCET is crucial in the chemistry of energy conversion such as water oxidation and CO_2 reduction.

ASSOCIATED CONTENT

Ⓢ Supporting Information

An example of energy gap integration, the data of the energy levels in Figure 1, and some PBE0 results. This material is available free of charge via the Internet at http://pubs.acs.org.

AUTHOR INFORMATION

Corresponding Authors

*E-mail: jcheng@abdn.ac.uk.
*E-mail: ms284@cam.ac.uk.

Notes

The authors declare no competing financial interest.

Biographies

Jun Cheng is currently a lecturer at the University of Aberdeen and previously was a junior research fellow at Emmanuel College at Cambridge. His research interest is computational and theoretical (photo)electrochemistry and catalysis.

Xiandong Liu is an associate professor at Nanjing University. He joined the Sprik group at Cambridge in 2012 to work on computational geochemistry of mineral interfaces and transition metal complexes.

Joost VandeVondele is currently an ERC funded assistant professor at the ETH Zurich. His research focusses on the development and application of new tools for the accurate simulation of large and complex systems, which are contributed to the community in the form of the CP2K simulation package.[7]

Marialore Sulpizi is a Junior Professor in the theory of Condensed Matter at the University of Mainz. Her current research interests focus on the understanding of microscopic properties at interfaces (including structure, spectroscopy, and reactivity) from DFTMD.

Michiel Sprik is Professor of Theoretical Chemistry at the University of Cambridge. After spending many years on studying the physical chemistry of aqueous solutions using DFTMD methods, he is now trying to extend these methods to interfacial electrochemistry.

ACKNOWLEDGMENTS

REFERENCES

(1) Tomasi, J.; Mennucci, B.; Cammi, R. Quantum Mechanical Continuum Solvation Models. *Chem. Rev.* **2005**, *105*, 2999−3094.

(2) Marenich, A. V.; Ho, J.; Coote, M. L.; Cramer, C. J.; Truhlar, D. G. Computational Electrochemistry: Prediction of Liquid-Phase Reduction Potentials. *Phys. Chem. Chem. Phys.* **2014**, *16*, 15068−15106 DOI: 10.1039/c4cp01572j.

(3) Warshel, A.; Sharma, P. K.; Kato, M.; Parson, W. A. Modelling Electrostatics Effects in Proteins. *Biochim. Biophys. Acta* **2006**, *1764*, 1647−1676.

(4) Kamerlin, S. C. L.; Haranczyk, M.; Warshel, A. Progress in Ab Initio QM/MM Free-Energy Simulations of Electrostatic Energies in Proteins: Accelerated QM/MM Studies of pKa, Redox Reactions and Solvation Free Energies. *J. Phys. Chem. B* **2009**, *113*, 1253−1272.

(5) Wang, L.-P.; Van Voorhis, T. A Polarizable QM/MM Explicit Solvent Model for Computational Electrochemistry in Water. *J. Chem. Theor. Comput.* **2012**, *8*, 610−617.

(6) VandeVondele, J.; Krack, M.; Mohamed, F.; Parrinello, M.; Chassaing, T.; Hutter, J. Quickstep: Fast and Accurate Density Functional Calculations Using a Mixed Gaussian and Plane Waves Approach. *Comput. Phys. Commun.* **2005**, *167*, 103−128.

(7) The CP2K developers group, http://www.cp2k.org, 2008.

(8) King, G.; Warshel, A. Investigation of the Free Energy Functions for Electron Transfer Reactions. *J. Chem. Phys.* **1990**, *93*, 8682−8692.

(9) Blumberger, J.; Tavernelli, I.; Klein, M. L.; Sprik, M. Diabatic Free Energy Curves and Coordination Fluctuations for the Aqueous Ag^+/Ag^{2+} Redox Couple: A Biased Born-Oppenheimer Molecular Dynamics Investigation. *J. Chem. Phys.* **2006**, *124*, No. 064507.

(10) Sulpizi, M.; Sprik, M. Acidity Constants from Vertical Energy Gaps: Density Functional Theory Based Molecular Dynamics Implementation. *Phys. Chem. Chem. Phys.* **2008**, *10*, 5238−5249.

(11) Cheng, J.; Sulpizi, M.; Sprik, M. Redox Potentials and pKa for Benzoquinone from Density Functional Theory Based Molecular Dynamics. *J. Chem. Phys.* **2009**, *131*, No. 154504.

(12) Costanzo, F.; Della Valle, R. G.; Sulpizi, M.; Sprik, M. The Oxidation of Tyrosine and Tryptophan Studied by a Molecular Dynamics Normal Hydrogen Electrode. *J. Chem. Phys.* **2011**, *134*, No. 244508.

(13) Adriaanse, C.; Cheng, J.; Chau, V.; Sulpizi, M.; VandeVondele, J.; Sprik, M. Aqueous Redox Chemistry and the Electronic Band Structure of Liquid Water. *J. Phys. Chem. Lett.* **2012**, *3*, 3411−3415.

(14) Sulpizi, M.; Sprik, M. Acidity Constants from DFT-Based Molecular Dynamics Simulations. *J. Phys.: Condens. Matter* **2010**, *22*, No. 284116.

(15) Mangold, M.; Rolland, L.; Costanzo, F.; Sprik, M.; Sulpizi, M.; Blumberger, J. Absolute pKa Values and Solvation Structure of Amino Acids from Density Functional Based Molecular Dynamics Simulation. *J. Chem. Theor. Comput.* **2011**, *7*, 1951−1961.

(16) Liu, X.; Sprik, M.; Cheng, J. Hydration, Acidity and Metal Complexing of Polysulfide Species: A First Principles Molecular Dynamics Study. *Chem. Phys. Lett.* **2013**, *563*, 9−14.

(17) Liu, X.; Cheng, J.; Sprik, M.; Lu, X. Solution Structures and Acidity Constants of Molybdic Acid. *J. Phys. Chem. Lett.* **2013**, *4*, 2926−2930.

(18) Cheng, J.; Sprik, M. Acidity of the Aqueous Rutile $TiO_2(110)$ Surface from Density Functional Theory Based Molecular Dynamics. *J. Chem. Theor. Comput.* **2010**, *6*, 880−889.

(19) Cheng, J.; Sprik, M. Aligning Electronic Energy Levels at the TiO_2/H_2O Interface. *Phys. Rev. B* **2010**, *82*, No. 081406(R).

(20) Cheng, J.; Sprik, M. Alignment of Electronic Energy Levels at Electrochemical Interfaces. *Phys. Chem. Chem. Phys.* **2012**, *14*, 11245−11267.

(21) Cheng, J.; Sulpizi, M.; VandeVondele, J.; Sprik, M. Hole Localization and Thermochemistry of Oxidative Dehydrogenation of Aqueous Rutile $TiO_2(110)$. *ChemCatChem* **2012**, *4*, 636−640.

(22) Sulpizi, M.; Gaigeot, M.-P.; Sprik, M. The Silica−Water Interface: How the Silanols Determine the Surface Acidity and Modulate the Water Properties. *J. Chem. Theor. Comput.* **2012**, *8*, 137−147.

(23) Tazi, S.; Rotenberg, B.; Salanne, M.; Sprik, M.; Sulpizi, M. Absolute Acidity of Clay Edge Sites from Ab-Initio Simulations. *Geochim. Cosmochim. Acta* **2012**, *94*, 1−11.

(24) Liu, X.; Cheng, J.; Sprik, M.; Lu, X.; Wang, R. Understanding Surface Acidity of Gibbsite with First Principles Molecular Dynamics Simulations. *Geochim. Cosmochim. Acta* **2013**, *120*, 487−495.

(25) Liu, X.; Lu, X.; Sprik, M.; Cheng, J.; Meijer, E. J.; Wang, R. Acidity of Edge Surface Sites of Montmorillonite and Kaolinite. *Geochim. Cosmochim. Acta* **2013**, *117*, 180−190.

(26) Mori-Sánchez, P.; Cohen, A. J.; Yang, W. Localization and Delocalization Errors in Density Functional Theory and Implications for Band-Gap Prediction. *Phys. Rev. Lett.* **2008**, *100*, No. 146401.

(27) Guidon, M.; Hutter, J.; VandeVondele, J. Auxiliary Density Matrix Methods for Hartree-Fock Exchange Correlations. *J. Chem. Theor. Comput.* **2010**, *6*, 2348−2364.

(28) Leslie, M.; Gillan, M. J. The Energy and Elastic Dipole Tensor of Defects in Ionic Crystals Calculated by the Supercell Method. *J. Phys.: Condens. Matter* **1985**, *18*, 973.

(29) Hummer, G.; Pratt, R. L.; Garcia, A. E. Free Energy of Ion Hydration. *J. Phys. Chem.* **1996**, *100*, 1206−1215.

(30) Lin, Y.-L.; Aleksandrov, A.; Simonson, T.; Roux, B. An Overview of Electrostatic Free Energy Computations for Solutions and Proteins. *J. Chem. Theor. Comput.* **2014**, *10*, 2690−2709.

(31) Freysoldt, C.; Grabowski, B.; Hickel, T.; Neugebauer, J.; Kresse, G.; Janoti, A.; VandeWalle, C. G. First-Principles Calculations of Point Defects in Solids. *Rev. Mod. Phys.* **2014**, *86*, 253−305.

(32) Komsa, H.-P.; Rantala, T. T.; Pasquarello, A. Finite-size Supercell Correction Schemes for Charged Defect Calculations. *Phys. Rev. B* **2012**, *86*, No. 045112.

(33) Ayala, R.; Sprik, M. A Classical Point Charge Model Study of System Size Dependence of Oxidation and Reorganization Free Energies in Aqueous Solution. *J. Phys. Chem. B* **2008**, *112*, 257−269.

(34) Pham, T. A.; Zhang, C.; Schwegler, E.; Galli, G. Probing the Electronic Structure of Water with Many-Body Perturbation Theory. *Phys. Rev. B* **2014**, *89*, No. 060202(R).

(35) Trasatti, S. The Absolute Electrode Potential: An Explanatory Note. *Pure Appl. Chem.* **1986**, *58*, 955−966.

(36) Warren, J. J.; Tronic, T. A.; Mayer, J. M. Thermochemistry of Proton-Coupled Electron Transfer Reagents and its Implications. *Chem. Rev.* **2010**, *110*, 6961−7001.

(37) Alkauskas, A.; Broqvist, P.; Pasquarello, A. Defect Levels through Hybrid Density Functionals: Insights and Applications. *Phys. Status Solidi B* **2011**, *248*, 775−789.

(38) Yang, W.; Cui, Q.; Min, D.; Li, H. In *Annual Reports in Computational Chemistry*; Wheeler, R. A., Ed.; Elsevier: Amsterdam, 2010; Vol. 6, pp 51−62.

(39) Krukau, A. V.; Vydrov, O. A.; Izmaylov, A. F.; Scuseria, G. E. Influence of the Exchange Screening Parameter on the Performance of Screened Hybrid Functionals. *J. Chem. Phys.* **2006**, *125*, No. 224106.

(40) Perdew, J. P.; Ernzerhof, M.; Burke, K. Rationale for Mixing Exact Exchange with Density Functional Approximations. *J. Chem. Phys.* **1996**, *105*, 9982−9985.

(41) Opalka, D.; Pham, T.; Sprik, M.; Galli, G. The Ionization Potential of Aqueous Hydroxide Computed Using Many-Body Perturbation Theory. *J. Chem. Phys.* **2014**, *141*, No. 034501.

(42) Del Ben, M.; Schönherr, M.; Hutter, J.; VandeVondele, J. Bulk Liquid Water at Ambient Temperature and Pressure from MP2 Theory. *J. Phys. Chem. Lett.* **2013**, *4*, 3753−3759.

(43) Del Ben, M.; Hutter, J.; VandeVondele, J. Electron Correlation in the Condensed Phase from a Resolution of Identity Approach Based on the Gaussian and Plane waves Scheme. *J. Chem. Theor. Comput.* **2013**, *9*, 2654−2671.